Journal of Materials Chemistry A

Accepted Manuscript

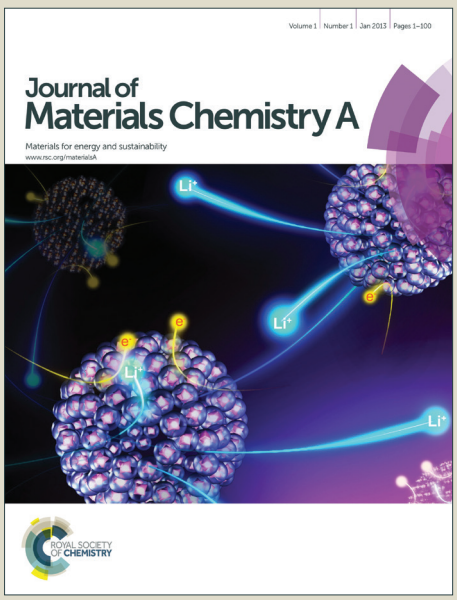

ROYAL SOCIETY OF CHEMISTRY

www.rsc.org/materialsA

TOC

Si/Ge Nanocomposite Prepared by One-step Solid-state Metathesis Reaction and Its Enhanced Electrochemical Performance

Ning Lin, Liangbiao Wang, Jianbin Zhou, Jie Zhou, Ying Han, Yongchun Zhu*, and Yitai Qian*

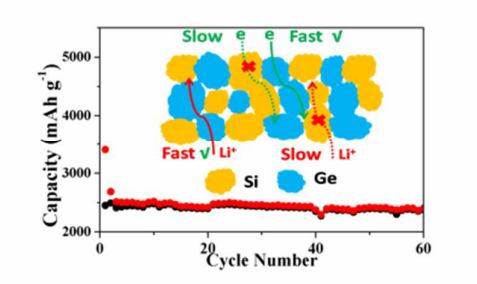

High-performance Si/Ge anode is prepared through one-step solid-state metathesis reaction between Mg_2Si and GeO_2 for the first time.

Journal Name

COMMUNICATION

Si/Ge Nanocomposite Prepared by One-step Solid-state Metathesis Reaction and Its Enhanced Electrochemical Performance

Received 00th January 20xx,
Accepted 00th January 20xx

DOI: 10.1039/x0xx00000x

www.rsc.org/

Ning Lin[a], Liangbiao Wang[a], Jianbin Zhou[a], Jie Zhou[a], Ying Han[a], Yongchun Zhu*[a], and Yitai Qian*[a]

Si/Ge nanocomposite composed of interconnected Si and Ge nanoparticles is prepared through one-step solid-state metathesis reaction between Mg_2Si and GeO_2 for the first time. As an anode, the Si/Ge electrode exhibits reversible capacity of 2404.7 mAh g^{-1} at 0.5 A g^{-1} over 60 cycles and long-term cycling stability with a capacity of 1260 mAh g^{-1} over 500 cycles even at 5 A g^{-1}.

Recently, Si and Ge, as two typical group IVA elements, based materials are considered as viable anode candidates for the next generation of rechargeable lithium ion batteries. [1-4] It has been demonstrated that Si anode displays the highest theoretical specific capacity of 3579 mAh g^{-1} and low working potential (< 0.5 V). [5, 6] Meanwhile, Ge based anode exhibits a specific capacity of 1384 mAh g^{-1}. Notably, the other appealing merits of Ge are the high lithium ion diffusivity (400 times faster than Si) and electrical conductivity (10^4 times higher than Si). [7-9] However, main challenge facing various alloy-type anode including Si and Ge is the drastic volume variation during lithiation/delithiation process, thus leading to rapid capacity fading upon cycling, [10, 11] which is urgent to be overcome.

To make full use of the merits of Si and Ge synchronously, hybrid structures contained Si and Ge have been designed to modify their physicochemical properties and thus enhance their lithium ion storage performance. [12] The Si component make a contribution to the higher specific capacity. The electric/ionic conductivity of Si/Ge composite could be greatly enhanced by the Ge element. It is well-accepted that some intermetallic compounds containing active anode materials could effectively accommodate the volume change due to the synergistic effect. [13] During lithiation process, Ge would start to react with lithium ion at around 0.5 V, followed by the lithiation reaction of both Ge and Si. [14, 15] As a result, strain stress generated by volume variation during Li-alloying process could be released gradually, thus maintaining the structural and electrical integrity of the electrode. To date, only a few fabrication techniques have been developed to prepare Si/Ge nanocomposite. For example, Si/Ge double-layered nanotube arrays, prepared by chemical vapor deposition (CVD), showed capacity retention of 1484 mAh g^{-1} at 0.2 C over 50 cycles. [8] Li et al. fabricated Si/Ge core–shell nanoarrays through radio frequency magnetron sputtering, which delivered a reversible capacity of 0.42 mAh cm^{-2} at a current density of 20 μA cm^{-2} after 60 cycles. [9] Si/Ge thin film, synthesized by evaporative deposition in high vacuum, exhibited enhanced rate performance due to the favorable electronic conductivity and ionic diffusivity of Ge component. [11] However, developing a simple chemical approach for fabricating Si/Ge composite remains a great challenge.

Typically, the metathesis reactions have been widely employed for preparing Si based materials, such as reacting Mg_2Si with $SiCl_4$ and silicon oxides, [15, 16] reacting ''Zintl phases'' (NaSi, KSi) together with metal halides or ammonium salts. [17, 18] Recently, our group reported the synthesis of Si nanoparticles anode by the metathesis reaction of Mg_2Si and $ZnCl_2$ ($Mg_2Si + ZnCl_2 \rightarrow MgCl_2 + Zn + Si$). [10]

In this study, inspired by the typical metathesis reaction, a one-step solid-state metathesis reaction between Mg_2Si (reductant) and GeO_2 (oxidant) is developed for preparing Si/Ge composite composed of interconnected Si and Ge nanoparticles. The employed reaction can be formulated as Equation 1.

$Mg_2Si + GeO_2 \rightarrow 2\ MgO + Ge + Si$, (1).

As anode for rechargeable lithium ion batteries, the obtained Si/Ge composite delivers a reversible capacity of 2404.7 mAh g^{-1} at 0.5 A g^{-1} after 60 cycles, fine rate capability with 414 mA h g^{-1} at 20 A g^{-1} and long-term cycling stability with a capacity of 1260 mAh g^{-1} even at 5 A g^{-1} after 500 cycles.

[a] *Hefei National Laboratory for Physical Science at Micro-scale, Department of Chemistry, University of Science and Technology of China, Hefei, Anhui 230026, P. R. China. E-mail: ychzhu@ustc .edu.cn; ytqian@ust c.edu.cn*

† Electronic Supplementary Information (ESI) available: Experimental section; auxiliary analysis such as TEM, EDS mapping images, and EIS data of the as-prepared samples.. See DOI: 10.1039/x0xx00000x

The contents of the raw product obtained from the Equation 1 without any washing treatment are determined by X-ray diffraction (XRD) analysis, as the blue line exhibited in the Figure 1a. The two peaks at around 43 and 78.5° are assigned to MgO (labeled as "◆" JCPDS No. 04-0829). The weak peak located at 40° is the characterization peak of cubic phase Mg_2Si (labeled as "★" JCPDS No. 34-0458), due to a small quantity of residual reactant. And the two amorphous peaks at around 31 and 36° are characterized as magnesium silicate (labeled as "▲" JCPDS No. 03-0174), which are attributed to the by-products. Notably, the main peaks of Si (labeled as "☆" JCPDS No. 77-2111) and Ge (labeled as "◇" JCPDS No. 03-0478) are clearly exhibited in the patterns. After washing treatment, these by-products are all removed, and well-crystalized Si and Ge appear in the composite, as shown in Figure 1a. Furthermore, the final Si/Ge composite is analyzed by Raman spectrum. Two clear peaks at 290 and 515 cm^{-1} correspond to first-order Raman scattering from optic phonons of Ge-Ge and Si-Si stretching motions, suggesting the existence of Si and Ge components, respectively. [19] Meanwhile, it should be pointed out that the weak peak located at around 400 cm^{-1} is attributed to Si-Ge bonds, which may be formed during the reaction procedure. [20] The molar ratio of Ge to Si is estimated to be about 1:0.78, determined by X-ray photoelectron emission microscopy. (Supporting Information)

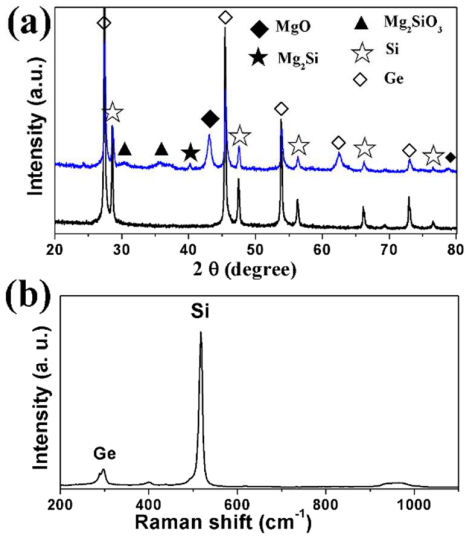

Figure 1. (a) XRD patterns of the crude product obtained from equation 1 (blue line), and the final product Si/Ge composite (black line). (b) Raman spectrum of as-prepared Si/Ge composite.

The morphology of the sample is investigated by electron microscopy images. Figure 2a shows the scanning electron microscope (SEM) image of the raw product. The bulk particle may compose of the above confirmed contents including MgO, Si, Ge and Mg_2SiO_3 that are aggregated together with dense surface. After removing the by-products, it can be seen that the final composite consists of disordered nano-particles (Figure 2b). Also, the transmission electron microscope (TEM) image, shown in Figure S 1, clearly exhibits the irregular structure with the overall size ranging from tens to over 100 nm. Furthermore, the energy-dispersive X-ray (EDX) spectroscopy mapping images were taken to determine the distribution state of Si and Ge components. Figure 2 c-e confirm that the Ge and Si nanoparticles are connected tightly. The corresponding high resolved TEM (HR-TEM) images (Figure 2f, g) show that a clear grain boundary between Si and Ge is formed. In addition, the mapping picture of the different particle, as exhibited in Figure S2, also presents the interconnected distribution of Si and Ge elements in the prepared Si/Ge composite. Base on the proposed Equation 1, it is reasonable to speculate that crystalline Si and Ge are generated simultaneously in the metathesis reaction system between Mg_2Si and GeO_2, facilitating the growth of the hybrid structure containing interconnected Si and Ge nanoparticles.

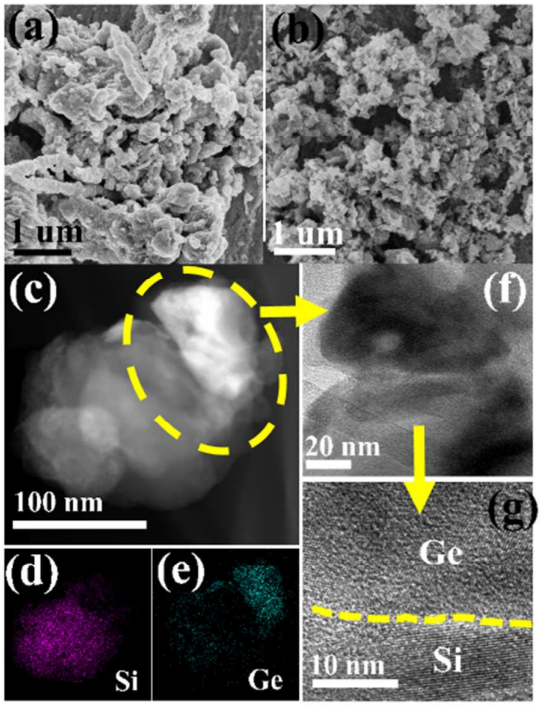

Figure 2. SEM images of (a) crude product, and (b) final Si/Ge composite. (c) TEM, (d) and (e) EDX mapping, (f) and (g) HR-TEM pictures of the Si/Ge composite.

As anode materials for rechargeable lithium ion batteries, the major electrochemical reactions of the prepared Si/Ge electrode during lithiation/delithiation process are investigated by cyclic voltammetry (CV), as shown in Figure 3a. In the first cycle, two cathodic peaks at 0.23 V and below 0.1 V are associated with the Li-alloying reactions of Ge and Si, and the formation of lithiated Si (Li_xSi) and Ge (Li_yGe), respectively. [21] In terms of anodic reactions, a sharp peak at 0.56 V is ascribed to the dealloying reaction of Li_yGe. The other two discrete peaks at 0.3 and 0.50 V correspond to the delithiation process of the Li_xSi. [11] In the second cycle, the lithiation peaks, exhibited in the first cycle, are shifted to higher voltage as a result of the transformation of Si or Ge from crystalline to amorphous phase during the first charging/discharging process. [11,20-22] Remarkably, the CV curves from 3rd to 10th cycles are overlapped very well, suggesting fine cycling stability.

Phase change of the Si/Ge electrode during the lithiation/delithiation process is further studied by the *ex situ* XRD analysis. Figure 3b exhibits the XRD patterns of untested Si/Ge electrode, three strong diffraction peaks at 43, 50.4, and 74.3° are assigned to the copper current collector (JCPDS No. 01-1242). [23] To avoid the interference of copper current collector, the strongest diffraction peaks of (111) plane of both Si and Ge are selected to study the phase change. During the first lithiation process, the diffraction intensity corresponding to Ge gradually becomes weak and diminishes while the potential is lower than 0.2 V (vs. Li/Li^+), which is caused by complete Li-alloying reaction of the Ge component. As keep on electrochemical lithiation, the CV curves indicate that the alloying reaction between Si and lithium ions is initiated. At 0.01 V, the residual peak implies the insufficient lithiation of Si during the first cycle. After five cycles, no obvious diffraction peak is observed, which may be resulted from the following two aspects. On one hand, the phases of Si and Ge transform from crystalized to amorphous structure completely after a few cycles. On the other hand, the generally lithiated phases, including crystalline Li_xSi and Li_yGe, are known to be metastable. Therefore, it will be difficult to observe these phases with *ex situ* characterization techniques.[24]

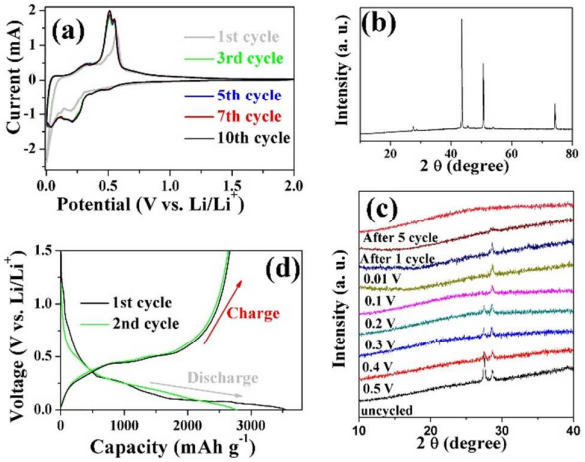

Figure 3. (a) CV curves of prepared Si/Ge electrode. (b) *ex situ* XRD patterns of Si/Ge electrode before cycled. (c) *ex situ* XRD patterns between 10 to 40° of Si/Ge electrodes discharged at different cut-off voltages, after 1 and 5 cycles at 0.5 A g^{-1}. (d) discharge/charge voltage plots of the Si/Ge electrode tested at 0.3 A g^{-1}.

Figure 3d exhibits the discharge/charge voltage profiles of Si/Ge electrode at a current density of 0.3 A g^{-1}. Two distinct voltage plateaus in the first discharge potential plateau are observed. According to the CV and *ex situ* XRD information, the plateau located at over 0.2 V and below 0.2 V may be mainly arisen from the lithiation of Ge and Si components, respectively. [8, 12] Notably, the first discharge and charge capacity are 3549 and 2639.3 mAh g^{-1}, corresponding to an initial coulombic efficiency of 74.4%. The irreversible capacity is likely resulted from the formation of solid electrolyte interface (SEI) membrane, irreversible reaction between Li^+ and Si/Ge, and the side reactions between the active material and the electrolyte (especially $LiPF_6$). [25] During the second cycle, the discharge potential plateau of first cycle is replaced by a sloping curve due to the amorphization process, which is consistent with the CV and *ex situ* XRD data.

Next, the cycling behavior of the as-prepared Si/Ge composite are monitored by galvanostatic charge/discharge tests. As shown in Figure 4a, the Si/Ge composite delivers a reversible capacity as high as 2404.7 mAh g^{-1} at 0.5 A g^{-1} over 60 cycles. Despite the capacity degradation within the first two cycles, the reversible capacity of the Si/Ge electrode retains over 96% of the third discharge capacity after 60 cycles. Remarkably, the corresponding coulombic efficiency quickly increases to 93.5 % for the second cycle and further reaches to a steady value about 99 % after several cycles.

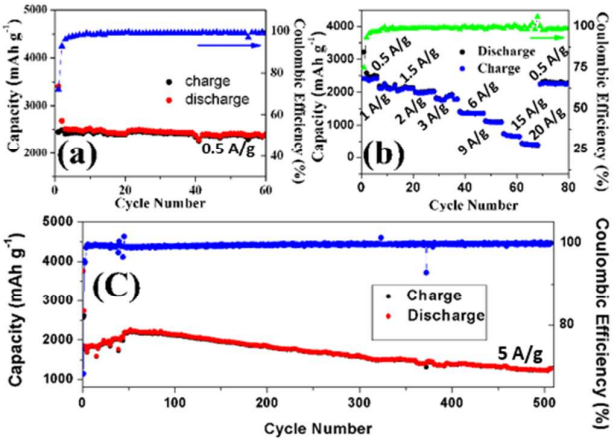

Figure 4. Galvanostatic discharge/charge measurements of the prepared Si/Ge electrode. Cycling performance tested at (a) 0.5 A g^{-1}, and (c) 5 A g^{-1}. (b) Rate capabilities at various current densities.

Moreover, the rate capability of the Si/Ge anode is investigated with increasing current densities from 0.5 to 20 A g^{-1}. As shown in Figure 4b, the Si/Ge anode exhibits the reversible capacity of 2422, 2186, 2143, 1986, 1803, 1365, 1099, 661, and 414 mA h g^{-1} at 0.5, 1.0, 1.5, 2, 3, 6, 9, 15, and 20 A g^{-1}, respectively. Importantly, when the current density is returned back to 0.5 A g^{-1} after cycling at high rate, stable capacity of 2266 mA h g^{-1} could still be resumed. Even at high current density, the corresponding coulombic efficiency is always over 98%, which is significant for practical application.

In addition, the long-term cycling stability at high current density electrode is elucidated, as shown in Figure 4c. It should be mentioned first that the cell is tested at a relative low current density of 0.3 A g^{-1} for first two cycles. The slight increase of capacity during the first 50 cycles may attribute to the gradually activation of Si/Ge at relatively high current density. [26] At higher current density of 5 A g^{-1}, the Si/Ge electrode displays a reversible capacity of 1260 mAh g^{-1} even over 500 cycles. And the corresponding coulombic efficiency maintains over 98% at 5 A g^{-1} except the relatively low value of the first cycle. The Nyquist plots, exhibited in Figure S3, indicates that the as-prepared Si/Ge electrode shows lower layer resistance than that of bare Si electrode. It is believed that the Ge component is helpful for improving the electron/ion transfer rate. Table S1 and Table S2

shows that the cycling stability and rate capability of the as-prepared Si/Ge composite is better than most previous Si/Ge composite.

The above impressive electrochemical performance of the as-prepared Si/Ge composite such as high reversible capacity, outstanding cycling stability and rate capability could be attributed to the unique structure with following features. Fundamentally, both Si (3579 mAh g^{-1}) and Ge (1380 mAh g^{-1}) are active, which guarantees the overall high specific capacity. More importantly, the key feature of the Si/Ge interconnected structure is the capability for overcoming the well-known pulverization problem facing Li-alloying materials, namely huge expansion and contraction, which is detrimental to the cycle life. As the lithium alloying/de-alloying reactions of Si and Ge proceed in a stepwise manner, the unreacted phases would serve as a buffer matrix to accommodate volume change generated by the reacted phases, thus releasing the mechanical strain and keeping the electrode structural integrity during repeated cycling. Furthermore, the Ge component, with higher electronic/ionic conductivity, provides a fast electron/ion diffusion path which ensures the sufficient lithiation/delithiation of the electrode during rapid discharge/charge cycling, thus maintaining high reversible capacity while increasing the current density.

Conclusions

In summary, Si/Ge nanocomposite composed of interconnected Si and Ge nanoparticles is fabricated through one-step, solid-state metathesis reaction between Mg_2Si and GeO_2 for the first time. This unique hybrid structure enables to take full advantages of inherent merits of both Si and Ge components such as high specific capacity and fast electronic/ionic diffusion. More importantly, the strain stress generated by huge volume variation is gradually released due to the different potential plateau of Si and Ge during lithiation/delithiation process. On basis of the above advantages, it is demonstrated here that the obtained Si/Ge anode is highly desirable for high performance rechargeable lithium ion batteries, such as high reversible capacity of 2404.7 mAh g^{-1}, good rate capability, and long-term cycling stability with a reversible capacity of 1260 mAh g^{-1} at 5 A g^{-1} even over 500 cycles.

Acknowledgements

This work was financially supported by the 973 Project of China (No. 2011CB935901), the National Natural Science Fund of China (No. 21471142, 21201158).

Notes and references

1 N. Lin, Y. Han, L. Wang, J. Zhou, J. Zhou, Y. C. Zhu, and Y. T. Qian, *Angew. Chem. Int. Ed.,* 2015, **54**, 3822–3825.
2 Z. L. Zhang, Y. H. Wang, W. F. Ren, Q. Q. Tan, Y. F. Chen, H. Li, Z. Y. Zhong and F. B. Su, *Angew. Chem.*, 2014, **126**, 5265-5269.
3 M-H. Park, Y-H. Cho, K. Kim, J. Kim, M. L. Liu, J. Cho, *Angew. Chem. Int. Ed.*, 2011, **50**, 9647-9650.
4 C. Wang, H. Wu, Z. Chen, M. T. McDowell, Y. Cui, Z. N. Bao, *Nat. Chem.*, 2013, **5**, 1042-1048.
5 X. Zhou, Y. X. Yin, L. J. Wan and Y. G. Guo, *Chem. Commun.*, 2012,**48**, 2198-2200.
6 M. Y. Wu, J. E. C. Sabisch, X. Y. Song, A. M. Minor, V. S. Battaglia, G. Liu, *Nano Lett.*, 2013, **13**, 5397-5402.
7 G. Jo, I. Choi, H. Ahn, M. J. Park, *Chem. Commun.*, 2012, **48**, 3987-3989.
8 T. Song, H. Y. Cheng, H. Choi, J-H. Lee, H. Han, D. H. Lee, D. S. Yoo, M-S. Kwon, J-M. Choi, S. G. Doo, H. Chang, J. L. Xiao, Y. G. Huang,W. I. Park, Y-C Chung, H. Kim, J. A. Rogers, U. Paik, *ACS Nano,* 2012, **6**, 303-309.
9 J. Li, C. Yue, Y. J. Yu, Y-S. Chui, J. Yin, Z. G. Wu, C. D. Wang, Y. S. Zang, W. Lin, J. T. Li, S. T. Wu, Q. H. Wu, *J. Mater. Chem. A*, 2013, **1**, 14344-14349.
10 L. B. Wang, N. Lin, J. B. Zhou, Y. C. Zhu and Y. T. Qian, *Chem. Commun.,* 2015, **51,** 2345-2348.
11 P. R. Abel, A. M. Chockla, Y-M. Lin, V. C. Holmberg, J. T. Harris, B. A. Korgel, A. Heller, C. Buddie Mullins, *ACS Nano,* 2013, **7**, 2249-2257.
12 T. Song, H. Y. Cheng, K. Town, H. Park, R. W. Black, S. Lee, W. I. Park, Y.G. Huang, J. A. Rogers, L. F. Nazar, U. Paik, *Adv. Funct. Mater.*, 2014, **24**, 1458-1464.
13 S. F. Fan, T. Sun, X. H Rui, Q. Y. Yan, H. H. Hng, *J. Power Sources,* 2012, **201**, 288-293.
14 C. K. Chan, X. F. Zhang, Y. Cui, *Nano. Lett.*, 2008, **8**, 307-309.
15 C. S. Yang, R. A. Bley, S. M. Kauzlarich, H. W. H. Lee and G. R. Delgado, *J. Am. Chem. Soc.*, 1999, **121**, 5191-5195.
16 Y. Hwa, W. S. Kim, B. C. Yu, J. H. Kim, S. H. Hong and H. J. Sohn, *J. Power Sources*, 2014, **252**, 144-149.
17 R. Epur, L. Minardi, M. K. Datta, S. J. Chung and P. N. Kumta, *J. Solid State Chem.*, 2013, **208**, 93-98.
18 K. A. Pettigrew, Q. Liu, P. P. Power and S. M. Kauzlarich, *Chem. Mater.*, 2003, **15**, 4005-4011.
19 M. I. Alonso, K. Winer, *Phys. Rev. B: Condens. Matter*, 1989, **39**, 10056-10063.
20 J. Z. Wang, N. Du, Z. Q. Song, H. Wu, H. Zhang, D. R. Yang, *J. Power Sources*, 2013, **229**, 185-189.
21 Y. Oumellal, N. Delpuech, D. Mazouzi, N. Dupre, J. Gaubicher, P. Moreau, P. Soudan, B. Lestriez , D. Guyomard, J. Mater. Chem., 2011, **21**, 6201-6208.
22 J. X. Yu, N. Du, H. Zhang. D. R. Yang, *RSC Adv.*, 2013, **3**, 7713-7717.
23 H. Kim, B. Han, J. Choo, J. Cho, *Angew. Chem. Int. Ed.*, 2008, **47**, 10151-10154.
24 C. K. Chan, H. L. Peng, G. Liu, K. McIlwrath, X. F. Zhang, R. A. Huggins, Y. Cui, *Nat. Nanotechnol.,* 2008, **3**, 31-35.
25 Y. J. Yu, C. Yue, S. B. Sun, W. Lin, H. Su, B. B. Xu, J. T. Li, S. T. Wu, J. Li, J. Y. Kang, *ACS Appl. Mater. Interfaces*, 2014, **6**, 5884-5890.
26 N. Lin, J. B. Zhou, Y. C. Zhu, Y. T. Qian, *J. Mater. Chem. A,* 2014, **2**, 19604-19608.